Nano Research 2015, 8(12): 3796–3802
DOI 10.1007/s12274-015-0878-8
Research Article
ISSN 1998-0124
CN 11-5974/O4

Piezoelectricity in two-dimensional group-III monochalcogenides

Wenbin Li[1] and Ju Li[1,2] (✉)

[1] *Department of Materials Science and Engineering, Massachusetts Institute of Technology, Cambridge, Massachusetts 02139, USA*
[2] *Department of Nuclear Science and Engineering, Massachusetts Institute of Technology, Cambridge, Massachusetts 02139, USA*

Received: 22 June 2015
Revised: 7 August 2015
Accepted: 10 August 2015

KEYWORDS
piezoelectricity, two-dimensional (2D) material, monochalcogenide, density functional theory (DFT) calculation

ABSTRACT

It is found that several layer-phase group-III monochalcogenides, including GaS, GaSe, and InSe, are piezoelectric in their monolayer form. First-principles calculations reveal that the piezoelectric coefficients of monolayer GaS, GaSe, and InSe (2.06, 2.30, and 1.46 pm·V^{-1}) are of the same order of magnitude as previously discovered two-dimensional (2D) piezoelectric materials such as boron nitride (BN) and MoS_2 monolayers. This study therefore indicates that a strong piezoelectric response can be obtained in a wide range of two-dimensional materials with broken inversion symmetry. The co-existence of piezoelectricity and superior photo-sensitivity in these monochalcogenide monolayer semiconductors means they have the potential to allow for the integration of electromechanical and optical sensors on the same material platform.

1 Introduction

Piezoelectric materials have a wide range of applications in systems that require robust electrical–mechanical coupling, which includes mechanical stress sensors, actuators, and energy harvesting devices [1–7]. However, technological progress continues to push for increasingly miniaturized devices, motivating a search for piezoelectric materials with a nanoscale form factor. For a crystal to be piezoelectric it is essential that it does not possess inversion symmetry [8]. Many layer-phase materials from which atom-thick two-dimensional (2D) materials [9] are derived have inversion symmetry in the bulk form. When thinned down to a monolayer, however, this inversion symmetry may no longer be present, meaning that the monolayers have the potential to become piezoelectric. Recently, 2D monolayers of boron nitride (BN) and some transition metal dichalcogenides (TMDCs) were theoretically predicted to be intrinsically piezoelectric with a large piezoelectric coefficient [10–12], an effect that has been experimentally demonstrated in the case of molybdenum disulfide (MoS_2) monolayers [6, 7, 13, 14]. The high crystal quality

Address correspondence to liju@mit.edu

and large elastic strain limits [15, 16] of such 2D materials could allow for the fabrication of high-performance nanoscale piezoelectric materials [6, 7], though it is believed that there are other 2D piezoelectric materials that have yet to be discovered. The identification and characterization of new 2D piezoelectric materials would not only expand the family of piezoelectric nanomaterials, but could also potentially introduce new phenomena and functionalities through a cross-coupling between electrical, chemical, optical, and mechanical responses.

2 Results and discussion

In this article, first-principles density functional theory (DFT) calculations are used to demonstrate that monolayers of group-III monochalcogenides (MX, M = Ga or In, X = S or Se) such as GaS, GaSe, and InSe are intrinsically piezoelectric and possess large piezoelectric coefficients. Bulk crystals of GaS, GaSe, and InSe share the same GaSe-type structure, which consists of vertically stacked X–M–M–X layers held together by weak van der Waals-like forces. Within each four-atom-thick monolayer, bonding is mainly covalent with some ionic characteristics. Depending on the stacking sequence of the monolayers, several different structural polytypes can exist and are defined as β, ε, γ, and δ phases [17]. In the past, these layered semiconductors attracted considerable attention by virtue of their nonlinear optical properties [18], and interest in MX was recently revived following the discovery that many layered compounds can be exfoliated down to monolayers with relative ease [9]. The study of 2D MX is now an active field of research, with monolayers or few-layers of all three compounds studied in this paper having either been mechanically exfoliated [19–24] or chemically synthesized via vapor phase transport [25, 26] and found to exhibit excellent potential for use in flexible photodetectors [20–23].

Figure 1 presents top and side views of the atomic structure of a GaS monolayer, which is representative of the monolayer structure in all three MX compounds studies here. Note that two vertically bonded layers of metal atoms are sandwiched between two layers of chalcogen atoms, and when viewed from the top, the M and X atoms each occupy one triangular sub-lattice

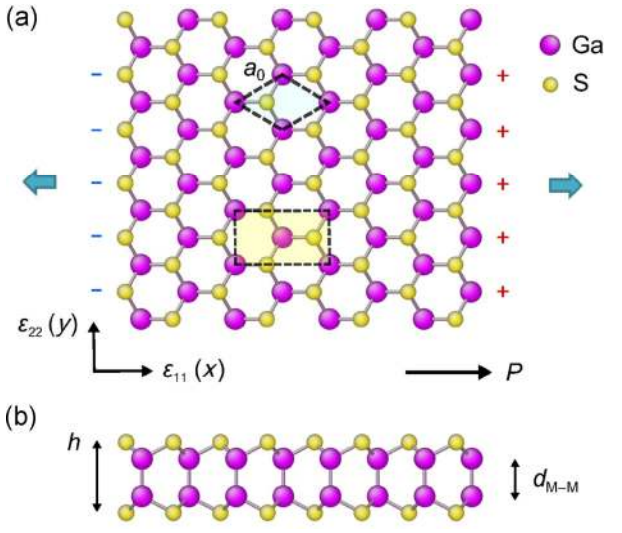

Figure 1 Structural model of a GaS monolayer viewed from (a) the top and (b) side. The larger-sized gallium atoms are purple, while the sulfur atoms are yellow. In (a), a two-dimensional primitive cell with rhombus shape and lattice constant a_0 is highlighted. The rectangular unit cell drawn beneath was used for DFT calculations. The x direction of the orthogonal coordinate system corresponds to the "armchair" direction of the monolayer, while the y direction corresponds to the "zigzag" direction. The direction of piezoelectric polarization after uniaxially stretching the monolayer along the x direction is labeled. In (b), the thickness of the monolayer, as defined by the distance between the top and bottom layer of sulfur atoms, is denoted by h. Also indicated is the distance between two bonded metal atoms, d_{M-M}.

of the overall honeycomb lattice. This structure of the MX monolayer therefore bears a strong similarity to monolayers of 2H-type TMDCs such as MoS_2. In fact, both MX and MoS_2 monolayers belong to the D_{3h} ($\bar{6}m2$) point group. A notable feature is the absence of an inversion center in the symmetry group, leading to a potential non-zero piezoelectric response in MX monolayers much like that seen in the case of BN and 2H-TMDC monolayers [6, 7, 10]. Consequently, first-principles calculations were first carried out to quantify the piezoelectric properties of the MX monolayers.

All DFT calculations were performed using the Vienna *ab initio* Simulation Package (VASP) with a plane wave basis set [27, 28] in accordance with the projector-augmented wave method [29]. Exchange-correlation functionals were used in the Perdew–Burke–Ernzerhof (PBE) form [30] within the generalized gradient approximation (GGA) [31]. For all calculations, the plane-wave cutoff energy was taken to be 450 eV. To facilitate the calculation of unit cell polarization,

an orthorhombic unit cell containing four M atoms and four X atoms was used, as indicated in Fig. 1(a). The cell height in the direction normal to the monolayer plane (*z* direction) was 20 Å. Brillouin zone integration employed an 11 × 18 × 1 *Γ*-centered Monkhorst–Pack [32] *k*-point grid, corresponding to *k*-point sampling spacing less than 0.1 $Å^{-1}$ along the reciprocal lattice vectors in the *x*–*y* plane. Convergence criteria for electronic and ionic relaxations were 10^{-6} eV and 10^{-3} eV·$Å^{-1}$, respectively.

Table 1 lists the DFT-optimized structural parameters, which includes the lattice constant a_0, monolayer thickness *h*, and M–M bond length $d_{M–M}$. Also included here are the corresponding experimental structural parameters for the bulk phase [17, 33, 34] to allow for direct comparison. The structural parameters obtained from the DFT calculations are in perfect agreement with a previous study [35]; their slightly greater magnitude compared to the bulk experimental values can be attributed to the use of a PBE exchange-correlation functional, which tends to overestimate lattice parameters by one or two percent [36]. As these materials are known semiconductors, the experimental bandgap values for the bulk phase and DFT calculated values for the monolayers are also listed in Table 1. These calculations indicated that all three MX compounds are indirect bandgap semiconductors in their monolayer form. The calculated bandgap values, however, are only provided for reference as the ground-state DFT calculations tend to significantly underestimate the bandgap value [37]. More accurate bandgap values for these monolayers have been obtained through excited-state calculations at the G_0W_0 [37, 38] level and hybrid functional calculations by Zhuang et al. [35].

To facilitate comparison with previously calculated results for 2D piezoelectric materials, the piezoelectric coefficients for the MX monolayers were calculated by following a procedure very similar to that used by Duerloo et al. [10]. To this end, the C_{11} and C_{12} planar elastic stiffness coefficients of the MX monolayers were first obtained by fitting the DFT-calculated unit-cell energy *U* to a series of 2D strain states (ε_{11}, ε_{22}) based on

$$C_{11}=\frac{1}{A_0}\frac{\partial^2 U}{\partial \varepsilon_{11}^2},\quad C_{22}=\frac{1}{A_0}\frac{\partial^2 U}{\partial \varepsilon_{22}^2},\quad C_{12}=\frac{1}{A_0}\frac{\partial^2 U}{\partial \varepsilon_{11}\partial \varepsilon_{22}} \tag{1}$$

where A_0 is the unit-cell area at zero strain. Since $C_{11} = C_{22}$ in the case of MX monolayers with D_{3h} point group symmetry, the small strain limit gives

$$\Delta u(\varepsilon_{11},\varepsilon_{22})=\frac{1}{2}C_{11}(\varepsilon_{11}^2+\varepsilon_{22}^2)+C_{12}\varepsilon_{11}\varepsilon_{22} \tag{2}$$

where

$$\Delta u(\varepsilon_{11},\varepsilon_{22})=[U(\varepsilon_{11},\varepsilon_{22})-U(\varepsilon_{11}=0,\varepsilon_{22}=0)]/A_0$$

is the change of unit-cell energy per area. Strain energy calculations were carried out on a 7 × 7 grid with ε_{11} and ε_{22} ranging from −0.006 to 0.006 in steps of 0.002. The atomic positions in the strained unit cell were allowed to fully relax, from which the experimentally relevant C_{11} and C_{12} relaxed-ion stiffness coefficients were determined. If the atomic positions are not allowed to relax after applying unit-cell strain, then the so-called clamped-ion coefficients (which are of theoretical interest) can also be calculated. Table 2 summarizes the clamped- and relaxed-ion stiffness coefficients for the three MX monolayers. In the relaxed-ion case, the Poisson ratios $v_\perp$ are also given, with these being obtained directly from the relaxed ion coordinates by evaluating the change in layer thickness that occurs

Table 1 Experimental and DFT-PBE calculated structural parameters and bandgap for bulk and monolayer MX. Values for the monolayer lattice constant a_0, monolayer thickness *h*, bond length between metal atoms $d_{M–M}$ and bandgap E_{gap} are listed

Material	Bulk experiment [17, 33, 34, 39]				Monolayer DFT-PBE calculation			
	a_0 (Å)	*h* (Å)	$d_{M–M}$ (Å)	E_{gap} (eV)	a_0 (Å)	*h* (Å)	$d_{M–M}$ (Å)	E_{gap} (eV)
GaS	3.59	4.60	2.45	2.59[a]	3.64	4.66	2.48	2.37
GaSe	3.76	4.78	2.46	2.10[b]	3.82	4.83	2.47	1.81
InSe	4.00	5.28	2.78	1.17[c]	4.09	5.39	2.82	1.40

[a,b,c] Bandgap values measured at *T* = 77, 4.2, and 300 K, respectively. Data is from Ref. [39].

Table 2 DFT-PBE calculated in-plane elastic stiffness C_{11} and C_{12} for monolayer MX. The Poisson ratio $v_{\perp}$ is also calculated for the relaxed-ion case

Material	Clamped-ion		Relaxed-ion		
	C_{11} (N·m^{-1})	C_{12} (N·m^{-1})	C_{11} (N·m^{-1})	C_{12} (N·m^{-1})	$v_{\perp}$
GaS	108	32	83	18	0.39
GaSe	91	26	70	16	0.34
InSe	75	35	51	12	0.40

in response to in-plane hydrostatic strain $\Delta h/h = -v_{\perp}(\varepsilon_{11}+\varepsilon_{22})$. The values of the relaxed-ion C_{11} coefficients show good agreement with an earlier calculation [35].

The linear piezoelectric coefficients of the MX monolayers were next calculated by evaluating the change in unit-cell polarization after imposing a uniaxial strain on the system, with this being based on the modern theory of polarization [40, 41] that is implemented in VASP. The polarization vector of the unit cell was obtained using the LCALCPOL tag in VASP. The linear piezoelectric coefficients $\boldsymbol{e}_{ijk}$ and $\boldsymbol{d}_{ijk}$ are third-rank tensors, as they relate the polarization vector $\boldsymbol{P}_i$, to the second-rank tensors of strain $\boldsymbol{\varepsilon}_{jk}$ and stress $\boldsymbol{\sigma}_{jk}$, respectively

$$\boldsymbol{e}_{ijk} = \frac{\partial \boldsymbol{P}_i}{\partial \boldsymbol{\varepsilon}_{jk}} \tag{3}$$

$$\boldsymbol{d}_{ijk} = \frac{\partial \boldsymbol{P}_i}{\partial \boldsymbol{\sigma}_{jk}} \tag{4}$$

Since the focus here is on quasi-2D systems, the i, j, and k indices can be considered as 1 or 2 and corresponding to the x or y directions defined in Fig. 1. The number of non-zero and unique piezoelectric coefficients is restricted by the symmetry elements of the crystal [8]. The symmetry of the piezoelectric properties of 2D monolayers with D_{3h} point group symmetry was analyzed by Duerloo et al. [10], who concluded that the only unique piezoelectric coefficients are e_{111} and d_{111}. Written in Voigt notation as e_{11} and d_{11}, these are further related through the elastic stiffness coefficients as

$$e_{11} = d_{11}(C_{11} - C_{22}) \tag{5}$$

The e_{11} piezoelectric coefficients of the MX monolayers were calculated by applying a uniaxial strain ε_{11} to the orthorhombic unit cell along the x direction, and then evaluating the differential change in unit-cell polarization per area along the x direction. The values of e_{11} reported here resulted from a linear fitting of the 2D polarization change ΔP_1 with respect to ε_{11} when ε_{11} was varied from –0.01 to 0.01 at intervals of 0.005, as illustrated in Fig. 2. Much like the evaluation of the elastic stiffness coefficients, the clamped-ion and relaxed-ion coefficients were obtained by changing whether the ionic positions were allowed to relax or not after applying strain. The relaxed-ion (or clamped-ion) d_{11} coefficients were then calculated from their corresponding e_{11} coefficients and elastic stiffness coefficients C_{11} and C_{12} using Eq. (5).

Table 3 lists the clamped-ion and relaxed-ion piezoelectric coefficients e_{11} and d_{11} that were calculated for the MX monolayers. The corresponding values for monolayer BN and MoS_2 calculated by Duerloo et al. [10] are also provided for comparison along with experimentally measured values of e_{11} for monolayer MoS_2 [7]. Benchmarking of the calculation for the MoS_2 monolayer produced excellent agreement with previous calculation results [10], with a 5% difference attributed to the use of different simulation packages and pseudopotentials. As can be seen from Table 3, the calculated relaxed-ion piezoelectric coefficients of the GaS and GaSe monolayers ($e_{11} = 1.34 \times 10^{-10}$ C·m^{-1},

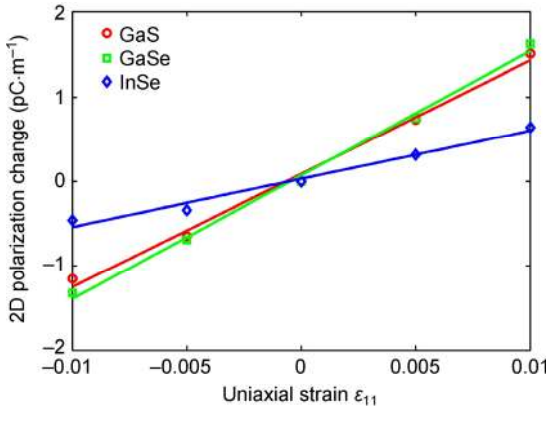

Figure 2 Change in unit-cell polarization of MX monolayers per unit of area along the x-direction after applying a uniaxial strain ε_{11} along the same direction. Ionic positions within the unit cells were relaxed after imposing this strain and the piezoelectric coefficients e_{11} corresponding to the slope of the lines were obtained through linear fitting.

Table 3 Calculated clamped-ion and relaxed-ion piezoelectric coefficients, e_{11} and d_{11}, of GaS, GaSe, and InSe monolayers. The piezoelectric coefficient of h-BN and MoS_2 monolayers calculated by Duerloo et al. [10], as well as the experimental value of e_{11} for MoS_2 monolayer [7], are listed for comparison

Material	Clamped-ion		Relaxed-ion	
	e_{11} (10^{-10} C·m^{-1})	d_{11} (pm·V^{-1})	e_{11} (10^{-10} C·m^{-1})	d_{11} (pm·V^{-1})
GaS	5.39	8.29	1.34	2.06
GaSe	5.22	9.67	1.47	2.30
InSe	5.17	13.26	0.57	1.46
h-BN cal. [10]	3.71	1.50	1.38	0.60
MoS_2 cal. [10]	3.06	2.91	3.64	3.73
MoS_2 exp. [7]			2.9	

d_{11} = 2.06 pm·V^{-1} and e_{11} = 1.47 × 10^{-10} C·m^{-1}, d_{11} = 2.30 pm·V^{-1}, respectively), are of the same order of magnitude as the MoS_2 monolayer (e_{11} = 3.64 × 10^{-10} C·m^{-1}, d_{11} = 3.73 pm·V^{-1}), and generally larger than the values for the BN monolayer (e_{11} = 1.38 × 10^{-10} C·m^{-1}, d_{11} = 0.60 pm·V^{-1}). The piezoelectric coefficients of the InSe monolayer (e_{11} = 0.57 × 10^{-10} C·m^{-1}, d_{11} = 1.46 pm·V^{-1}) are smaller than the GaS and GaSe monolayers, but still comparable to the BN monolayer. In contrast to the MoS_2 monolayer though, relaxing ion positions after applying strain significantly reduces the polarization of the MX monolayer, a trend that is more consistent with the BN monolayer. As a result, the clamped-ion piezoelectric coefficients of the MX monolayers are much larger than the relaxed-ion coefficients.

It is worth noting here that previous experimental studies have demonstrated that the piezoelectric coefficients of MoS_2 monolayer experience a non-monotonic decrease with an increasing number of layers, which is the result of breakage and the recovery of inversion symmetry with odd and even numbers of layers [6, 7]. This effect is considered likely to also exist in the MX monolayers due to the similarity in the layer-stacking sequence between bulk MX and MoS_2.

From an application perspective, experimental studies have demonstrated that monolayer or few-layer MX has superior photo-responsivity and a faster response time than MoS_2 monolayers [20–23]. Although the piezoelectric coefficients of MX monolayers are slightly smaller than those of MoS_2 monolayers, the piezoelectric properties of MX monolayers can nonetheless find application in situations where excellent photo-sensitivity and electro-mechanical coupling are both valued. For example, MX monolayers can be used to make flexible photodetectors in which both mechanical and optical signals can be electrically sensed using the same active material.

3 Conclusions

This study has computationally demonstrated that several single-layer group-III monochalcogenides (namely GaS, GaSe, and InSe) are not only piezoelectric, but have linear piezoelectric coefficients that are of the same order of magnitude as other 2D piezoelectric materials. These good piezoelectric properties, combined with the excellent photo-sensitivity of these 2D semiconductors, opens the possibility of integrating stress sensors, photo detectors and possibly even nano-scale transducers into the same 2D material platform, with potential applications in flexible electronics, optoelectronics and electromechanical systems.

Acknowledgements

We gratefully acknowledge financial support by National Science Foundation (No. DMR-1410636). Computational time on the Extreme Science and Engineering Discovery Environment (XSEDE) (No. TG-DMR130038) is gratefully acknowledged.

Electronic Supplementary Material: Supplementary material (atomic structures of the monolayers of GaS, GaSe, and InSe in the VASP/POSCAR format) is available in the online version of this article at http://dx.doi.org/10.1007/s12274-015-0878-8.

References

[1] Kingon, A. I.; Srinivasan, S. Lead zirconate titanate thin films directly on copper electrodes for ferroelectric, dielectric and piezoelectric applications. *Nat. Mater.* **2005**, *4*, 233–237.

[2] Nguyen, T. D.; Deshmukh, N.; Nagarah, J. M.; Kramer, T.; Purohit, P. K.; Berry, M. J.; McAlpine, M. C. Piezoelectric nanoribbons for monitoring cellular deformations. *Nat. Nanotechnol.* **2012**, *7*, 587–593.

[3] Wang, Z. L.; Song, J. H. Piezoelectric nanogenerators based on zinc oxide nanowire arrays. *Science* **2006**, *312*, 242–246.

[4] Yang, R. S.; Qin, Y.; Dai, L. M.; Wang, Z. L. Power generation with laterally packaged piezoelectric fine wires. *Nat. Nanotechnol.* **2009**, *4*, 34–39.

[5] Lee, E.; Park, J.; Yim, M.; Kim, Y.; Yoon, G. Characteristics of piezoelectric ZnO/AlN-stacked flexible nanogenerators for energy harvesting applications. *Appl. Phys. Lett.* **2015**, *106*, 023901.

[6] Wu, W. Z.; Wang, L.; Li, Y. L.; Zhang, F.; Lin, L.; Niu, S. M.; Chenet, D.; Zhang, X.; Hao, Y. F.; Heinz, T. F. et al. Piezoelectricity of single-atomic-layer MoS_2 for energy conversion and piezotronics. *Nature* **2014**, *514*, 470–474.

[7] Zhu, H. Y.; Wang, Y.; Xiao, J.; Liu, M.; Xiong, S. M.; Wong, Z. J.; Ye, Z. L.; Ye, Y.; Yin, X. B.; Zhang, X. Observation of piezoelectricity in free-standing monolayer MoS_2. *Nat. Nanotechnol.* **2015**, *10*, 151–155.

[8] Nye, J. F. *Physical Properties of Crystals: Their Representation by Tensors and Matrices*; Clarendon Press: Oxford, UK, 1957.

[9] Novoselov, K. S.; Jiang, D.; Schedin, F.; Booth, T. J.; Khotkevich, V. V.; Morozov, S. V.; Geim, A. K. Two-dimensional atomic crystals. *Proc. Natl. Acad. Sci. USA* **2005**, *102*, 10451–10453.

[10] Duerloo, K. A. N.; Ong, M. T.; Reed, E. J. Intrinsic piezoelectricity in two-dimensional materials. *J. Phys. Chem. Lett.* **2012**, *3*, 2871–2876.

[11] Michel, K. H.; Verberck, B. Theory of elastic and piezoelectric effects in two-dimensional hexagonal boron nitride. *Phys. Rev. B* **2009**, *80*, 224301.

[12] Qi, J. S.; Qian, X. F.; Qi, L.; Feng, J.; Shi, D. N.; Li, J. Strain-engineering of band gaps in piezoelectric boron nitride nanoribbons. *Nano Lett.* **2012**, *12*, 1224–1228.

[13] Reed, E. J. Piezoelectricity: Now in two dimensions. *Nat. Nanotechnol.* **2015**, *10*, 106–107.

[14] Wu, T.; Zhang, H. Piezoelectricity in two-dimensional materials. *Angew. Chem., Int. Ed.* **2015**, *54*, 4432–4434.

[15] Lee, C.; Wei, X. D.; Kysar, J. W.; Hone, J. Measurement of the elastic properties and intrinsic strength of monolayer graphene. *Science* **2008**, *321*, 385–388.

[16] Bertolazzi, S.; Brivio, J.; Kis, A. Stretching and breaking of ultrathin MoS_2. *ACS Nano* **2011**, *5*, 9703–9709.

[17] Kuhn, A.; Chevy, A.; Chevalier, R. Crystal structure and interatomic distances in GaSe. *Phys. Status Solidi A* **1975**, *31*, 469–475.

[18] Allakhverdiev, K. R.; Yetis, M. Ö.; Özbek, S.; Baykara, T. K.; Salaev, E. Y. Effective nonlinear GaSe crystal. Optical properties and applications. *Laser Phys.* **2009**, *19*, 1092–1104.

[19] Late, D. J.; Liu, B.; Matte, H. S. S. R.; Rao, C. N. R.; Dravid, V. P. Rapid characterization of ultrathin layers of chalcogenides on SiO_2/Si substrates. *Adv. Funct. Mater.* **2012**, *22*, 1894–1905.

[20] Hu, P. A.; Wen, Z. Z.; Wang, L. F.; Tan, P. H.; Xiao, K. Synthesis of few-layer GaSe nanosheets for high performance photodetectors. *ACS Nano* **2012**, *6*, 5988–5994.

[21] Hu, P. A.; Wang, L. F.; Yoon, M.; Zhang, J.; Feng, W.; Wang, X. N.; Wen, Z. Z.; Idrobo, J. C.; Miyamoto, Y.; Geohegan, D. B. et al. Highly responsive ultrathin GaS nanosheet photodetectors on rigid and flexible substrates. *Nano Lett.* **2013**, *13*, 1649–1654.

[22] Lei, S. D.; Ge, L. H.; Najmaei, S.; George, A.; Kappera, R.; Lou, J.; Chhowalla, M.; Yamaguchi, H.; Gupta, G.; Vajtai, R. et al. Evolution of the electronic band structure and efficient photo-detection in atomic layers of InSe. *ACS Nano* **2014**, *8*, 1263–1272.

[23] Tamalampudi, S. R.; Lu, Y. Y.; Kumar, U. R.; Sankar, R.; Liao, C. D.; Moorthy, B. K.; Cheng, C. H.; Chou, F. C.; Chen, Y. T. High performance and bendable few-layered InSe photodetectors with broad spectral response. *Nano Lett.* **2014**, *14*, 2800–2806.

[24] Sánchez-Royo, J. F.; Muñoz-Matutano, G.; Brotons-Gisbert, M.; Martínez-Pastor, J. P.; Segura, A.; Cantarero, A.; Mata, R.; Canet-Ferrer, J.; Tobias, G.; Canadell, E. et al. Electronic structure, optical properties, and lattice dynamics in atomically thin indium selenide flakes. *Nano Res.* **2014**, *7*, 1556–1568.

[25] Lei, S. D.; Ge, L. H.; Liu, Z.; Najmaei, S.; Shi, G.; You, G.; Lou, J.; Vajtai, R.; Ajayan, P. M. Synthesis and photoresponse of large GaSe atomic layers. *Nano Lett.* **2013**, *13*, 2777–2781.

[26] Zhou, Y. B.; Nie, Y. F.; Liu, Y. J.; Yan, K.; Hong, J. H.; Jin, C. H.; Zhou, Y.; Yin, J. B.; Liu, Z. F.; Peng, H. L. Epitaxy and photoresponse of two-dimensional GaSe crystals on flexible transparent mica sheets. *ACS Nano* **2014**, *8*, 1485–1490.

[27] Kresse, G.; Furthmüller, J. Efficiency of *ab-initio* total energy calculations for metals and semiconductors using a plane-wave basis set. *Comput. Mater. Sci.* **1996**, *6*, 15–50.

[28] Kresse, G.; Furthmuller, J. Efficient iterative schemes for *ab initio* total-energy calculations using a plane-wave basis set. *Phys. Rev. B* **1996**, *54*, 11169–11186.

[29] Blöchl, P. E. Projector augmented-wave method. *Phys. Rev. B* **1994**, *50*, 17953–17979.

[30] Perdew, J. P.; Burke, K.; Ernzerhof, M. Generalized gradient approximation made simple. *Phys. Rev. Lett.* **1996**, *77*, 3865–3868.

[31] Perdew, J. P.; Chevary, J. A.; Vosko, S. H.; Jackson, K. A.; Pederson, M. R.; Singh, D. J.; Fiolhais, C. Atoms, molecules, solids, and surfaces: Applications of the generalized gradient approximation for exchange and correlation. *Phys. Rev. B* **1992**, *46*, 6671–6687.

[32] Monkhorst, H. J.; Pack, J. D. Special points for brillouin-zone integrations. *Phys. Rev. B* **1976**, *13*, 5188–5192.

[33] Kuhn, A.; Chevy, A.; Chevalier, R. Refinement of 2H GaS β-type. *Acta Cryst. B* **1976**, *32*, 983–984.

[34] Rigoult, J.; Rimsky, A.; Kuhn, A. Refinement of the 3R γ-indium monoselenide structure type. *Acta Cryst. B* **1980**, *36*, 916–918.

[35] Zhuang, H. L.; Hennig, R. G. Single-layer group-III monochalcogenide photocatalysts for water splitting. *Chem. Mater.* **2013**, *25*, 3232–3238.

[36] Staroverov, V. N.; Scuseria, G. E.; Tao, J. M.; Perdew, J. P. Tests of a ladder of density functionals for bulk solids and surfaces. *Phys. Rev. B* **2004**, *69*, 075102.

[37] Hybertsen, M. S.; Louie, S. G. First-principles theory of quasiparticles: Calculation of band gaps in semiconductors and insulators. *Phys. Rev. Lett.* **1985**, *55*, 1418–1421.

[38] Hedin, L. New method for calculating the one-particle Green's function with application to the electron-gas problem. *Phys. Rev.* **1965**, *139*, A796–A823.

[39] Madelung, O. *Semiconductors: Data Handbook*; Springer-Verlag: New York, 2004.

[40] Kingsmith, R. D.; Vanderbilt, D. Theory of polarization of crystalline solids. *Phys. Rev. B* **1993**, *47*, 1651–1654.

[41] Resta, R.; Vanderbilt, D. *Physics of Ferroelectrics: A Modern Perspective*; Springer-Verlag: Berlin, 2007.